Geothermal Influence on the Hydrochemistry of Surface Streams in Patagonia Neuquina

Esteban Villalba, Lucía Santucci, Guido Borzi, Andrea I. Pasquini, Gerardo Páez, and Eleonora Carol

Abstract The Domuyo System Natural Protected Area in the Patagonia neuquina presents a mountainous relief with steep valleys carved by both, glacial and fluvial processes, where the main water courses are the streams named Manchana Covunco, Aguas Calientes and Covunco, which are tributaries of the Varvarco River. These streams run through an area of intense geothermal manifestations composed by aqueous solutions of high temperature, which determine the chemistry of streams and springs. The surface water courses and springs located upstream the thermal springs are neutral to alkaline, of low temperature and electric conductivity, and Ca-HCO_3/Ca-HCO_3-SO_4 types, respectively. Downstream the thermal springs, an increase in pH, temperature, and electrical conductivity is registered, as well as changes towards Na-Cl facies, the dominant composition of the thermal springs. Also, thermal springs increase the As content limiting the water potability. The contribution from thermal springs to streams varies between 24 and 47%, while in springs it is close to 10%. In addition to the mixing water, carbonate, plagioclase, and pyroxene weathering processes are mainly evidenced in both, thermal springs and springs, while surface water is associated with carbonate and gypsum-anhydrite dissolution. The dissolved REE contents are 10^4–10^7 times lower than the Upper Continental Crust and show a decrease downstream the geothermal field. Understanding the processes that determine the hydrochemistry is of great relevance in this type of arid mountainous environments with scarce knowledge.

E. Villalba (✉) · L. Santucci · G. Borzi · E. Carol (✉)
Centro de Investigaciones Geológicas, Universidad Nacional de la Plata, Consejo Nacional de Investigaciones Científicas y Técnicas, La Plata, Argentina
e-mail: evillalba@cig.museo.unlp.edu.ar

E. Carol
e-mail: eleocarol@fcnym.unlp.edu.ar

A. I. Pasquini
Centro de Investigaciones en Ciencias de La Tierra, Universidad Nacional de Córdoba, Consejo Nacional de Investigaciones Científicas y Técnicas, Córdoba, Argentina

G. Páez
Instituto de Recursos Minerales, Universidad Nacional de la Plata, Consejo Nacional de Investigaciones Científicas y Técnicas, La Plata, Argentina

A. I. Torres and V. A. Campodonico (eds.), *Environmental Assessment of Patagonia's Water Resources*, Environmental Earth Sciences,
https://doi.org/10.1007/978-3-030-89676-8_3

Keywords Geothermal system · Chemistry signature · Water courses · Springs

1 Introduction

In the central-west and northwestern region of Argentina, there are a large number of **hydrothermal manifestations**. Particularly in Patagonia, the main hydrothermal manifestations, in terms of their magnitude, are found in the Neuquén province (Mas 2010; Burd et al. 2014; Monasterio et al. 2017). These manifestations are represented by the Copahue-Caviahue volcano-hydrothermal system in the center-west area of Patagonia and the Domuyo geothermal system in the northwest of the aforementioned province (e.g. Agusto 2011; Chiodini et al. 2014).

The Domuyo System Natural Protected Area comprises a region dominated by Cenozoic volcanism represented by pyroclastic rocks, lavas and extrusive **domes** of rhyolitic and andesitic compositions (Fig. 1a). This felsic volcanism is found on a pre-volcanic Mesozoic basement composed of conglomerates, sandstones and pelitic rocks, which in turn lies on top of granites and granodiorites of Paleozoic age (Zanettini et al. 2001; Miranda et al. 2006; Pesce 2013; Galetto et al. 2018). The Domuyo System Natural Protected Area hosts the Domuyo Geothermal Field, which is located in the western sector of the Chos Malal fold and thrust belt. It has been

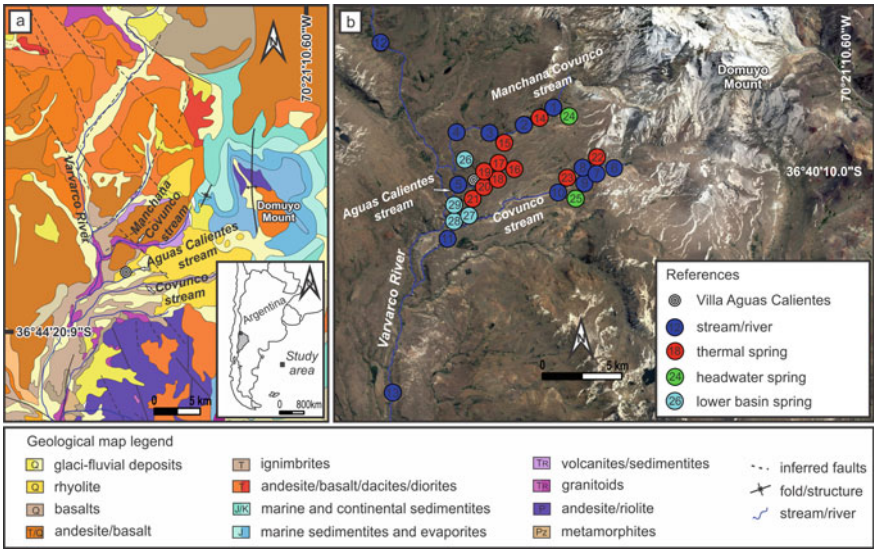

Fig. 1 **a** Regional geological map based on Zanettini et al. (2001), in the inset the Neuquén province is highlighted in grey color within the Argentina map and, **b** Satellite image from Google Earth Pro of the Domuyo system natural protected areas showing the location of sampling points from thermal springs (red points), surface water (blue points), and springs (green and light blue points). Capital letters are Quaternary (Q), Tertiary (T), Cretaceous (K), Jurassic (J), Triassic (TR), Permian (P) and Paleozoic age (Pz)

defined as a faulting-controlled **geothermal system**, where one of the most relevant tectonic structures is the Manchana Covunco Fault, whose location is close to the foot of the Domuyo Mount with a NNW-SSE direction (Galetto et al. 2018) and controls the location of the hydrothermal system. This region presents mountainous relief with steep valleys carved by both, glacial and fluvial processes (Zanettini et al. 2001). The main water courses are the streams named Manchana Covunco, Aguas Calientes and Covunco, which are tributaries of the Varvarco River (Fig. 1b). It is worth noting that small tributaries that drain through gullies and reach those streams are born in **springs**. At the same time, the area is characterized by the presence of **geothermal manifestations** composed of aqueous solutions of high temperature (from 40 to 97 °C), which result from ascending convective circulation of groundwater, mainly of **meteoric origin**, through fracture systems and permeable layers (Panarello et al. 1992; Chiodini et al. 2014; Tassi et al. 2016).

The climate is cold (annual average temperature close to 11 °C) and arid, with precipitation (200 mm per year) concentrated during austral winter, which occurs mainly in the form of snow (Pesce 2013; Cogliati et al. 2018). Therefore, in this region of arid characteristics, where water availability is scarce, streams and springs represent systems of high relevance as they constitute one of the main sources of water supply for the native fauna, livestock, and local inhabitants.

2 Field Methodology and Laboratory Analysis

In advance of carrying out field tasks for this study, antecedent information and satellite images were analyzed to design a monitoring network. Subsequently, samples of thermal water, springs and water courses were extracted underneath standardized norms of the American Public Health Association (APHA 2015) and analyzed in the Centro de Investigaciones Geológicas (CIG) laboratory. In the field, pH, electrical conductivity (EC), and temperature (T) of the water samples were measured with multiparameter equipment. Aliquots for Arsenic (As) and **rare earth elements (REE)** determinations (15 ml) were acidified to pH < 2 with ultrapure HNO_3 (>99.999%, redistilled) and stored in pre-cleaned polyethylene bottles. As and REE, from lanthanum (La) to lutetium (Lu), were determined by inductively coupled plasma-mass spectrometry (ICP-MS). Calibration curves were constructed from multi-element calibration standards (Perkin Elmer Inc. brand). All standard solutions and reagent blanks were prepared with deionized water and acidified with 1% HNO_3. The standard readings were repeated after measuring 5 samples. Aliquots of 1000 ml were stored in polyethylene bottles, without acidifying, at 4 °C for the determination of major ions.

Determinations of major ions (CO_3^{-2}, HCO_3^{-}, Cl^{-}, SO_4^{-2}, Ca^{+2}, Mg^{+2}, Na^{+}, K^{+}) were performed following standard methods outlined by APHA (2015). Carbonate (CO_3^{-2}), bicarbonate (HCO_3^{-}), calcium (Ca^{+2}), magnesium (Mg^{+2}), and chloride (Cl^{-}), were determined by volumetric methods (titration). The sodium (Na^{+}) and potassium (K^{+}) ions were determined by flame photometry, while sulfate (SO_4^{-2})

was precipitated in an acetic acid medium with $BaCl_2$ and its concentration was determined by turbidimetry. Ion balances were typically lower than 15% in all cases.

The chemical data of the waters were processed by into the Diagrammes Software (Smiler 2009), which was used to determine the different types of facies based on the major ion content and Piper (1944) diagram. Likewise, this software was used to estimate the saturation indices (SI) concerning different mineral phases using the Phreeqc Software (Parkhurst and Appelo 1999), which is incorporated into the program as an interface. In selected samples, the REE values obtained were normalized with respect to the concentration of the Upper Continental Crust (UCC) according to McLennan (2001). Finally, end-members mixing analyses were performed using Cl^- concentration in each type of sample because this is considered as a conservative ion and a useful tool to estimate, in this case, the contribution of **thermal springs** on the water courses and springs in the lower basin of the geothermal field.

3 Chemical Characteristics of Streams

The west flank of the Domuyo Mount presents a geothermal area that is crossed by the **watersheds** of the Manchana Covunco, Aguas Calientes, and Covunco (Figs. 1 and 2) which register an average low flow of 0.81 $m^3\ s^{-1}$. Table 1 shows the physicochemical parameters, the major composition, As content and relevant saturation indices of water samples. Springs in the headwater areas that contribute to the streams (samples 24 and 25; Fig. 1b) are characterized by an average pH, T, and EC of 7.2, 10.1 °C and 32 $\mu S\ cm^{-1}$ respectively, and Ca-HCO_3 facies (Fig. 3). At the **headwater** of the Manchana Covunco stream (sample 1; Figs. 1b and 2b), a pH of 8.1, temperature of 20.5 °C, and an EC of 1386 $\mu S\ cm^{-1}$ were recorded, and the chemical composition is dominated by Ca-HCO_3-SO_4 facies (Fig. 3). In the headwater of the Covunco stream (sample 6; Fig. 1b) pH values of 8.0, temperature of 15 °C and EC of 817 $\mu S\ cm^{-1}$ were registered, with Ca-HCO_3-SO_4-Cl facies (Fig. 3). In the middle watershed of the Manchana Covunco and Covunco streams and in the Aguas Calientes stream, numerous thermal springs are observed on the stream banks (Fig. 1b). These thermal springs have predominantly Na-Cl facies (Fig. 3), relatively high EC (from 1391 to 4394 $\mu S\ cm^{-1}$) and pH values between 7.2 and 9.3.

Downstream of the thermal springs, surface water of streams shows changes in the **chemical facies**, being predominantly Na-Cl (Fig. 3) and registering a strong increase of EC with respect to the values measured in the headwaters. The surface water collected from the Manchana Covunco stream (samples 2, 3, and 4; Figs. 1b and 2a) present average values of pH, temperature, and EC of 8.1, 28.7 °C and 3610 $\mu S\ cm^{-1}$ respectively. In the same way, waters from the Covunco stream (samples 7, 8, 9, 10 and 11; Figs. 1b and 2c, d) show a mean pH, temperature and EC of 8.4, 26.6 °C and 2856 $\mu S\ cm^{-1}$ respectively. In these areas of the low basin, several springs were also recognized, draining towards the streams (samples 26 to 29). These

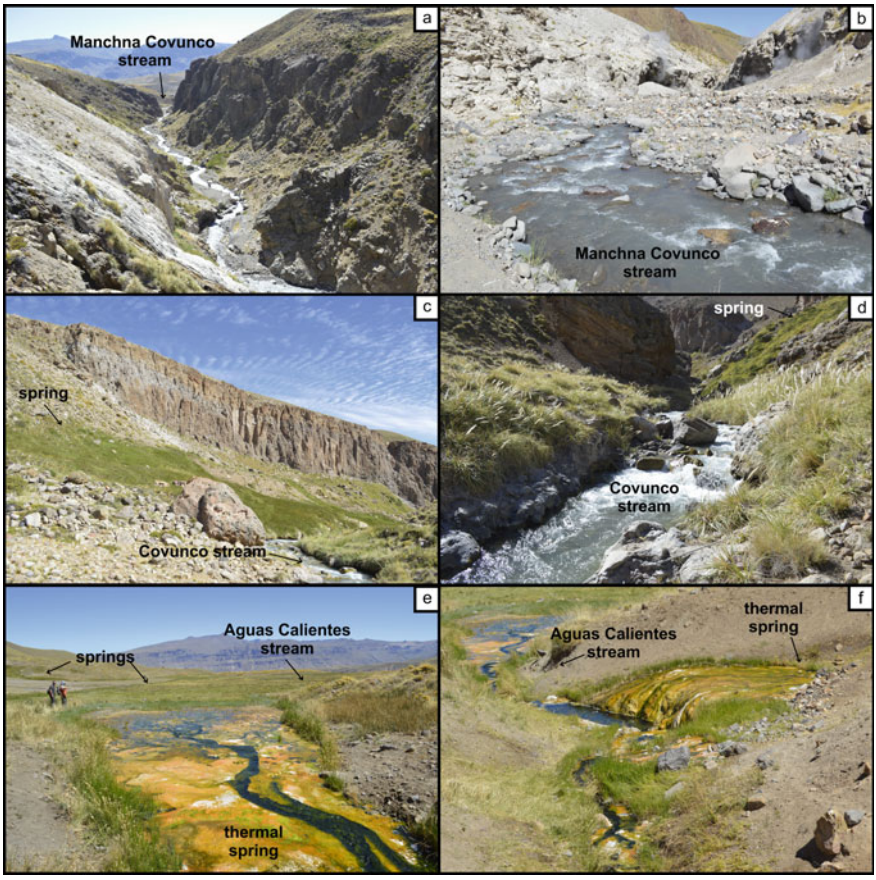

Fig. 2 Field photographs of surface water courses: Manchana Covunco stream in (**a**) and (**b**), Covunco stream in (**c**) and (**d**), Aguas Calientes stream in (**e**) and (**f**), springs in (**c**) to (**e**), and thermal springs in (**e**) and (**f**). Note headwaters are present in some water courses (white arrows)

waters present mean values of pH, temperature and EC of 7.1, 21.0 °C and 994 μS cm^{-1} respectively, while their chemical composition is Na-Cl (Table 1, Fig. 3).

The watersheds described above (Manchana Covunco and Covunco) drain towards the Varvarco River, which registers pH values of 7.94, temperature of 18.1 °C and EC of 320 μS cm^{-1} **upstream** the geothermal field (sample 12), while downstream the geothermal field (sample 13) the same parameters were of 7.80, 14.6 °C and 733 μS cm^{-1}, respectively. The chemical facies in Varvarco River is Ca-SO_4 in the upstream stretch and Na-SO_4-Cl after receiving the discharges from the geothermal field watersheds (Table 1, Fig. 3).

The joint analysis of all samples using the Piper (1944) diagram (Fig. 3) clearly shows the different evolution of chemical facies from the headwaters to the low basin, between surface water and springs (blue and green arrows, respectively, Fig. 3). In

Table 1 Physico-chemical parameters and major composition of water samples. Arsenic dissolved concentrations, as well as saturation indices (SI) of selected minerals are also included. Sample numbers are the same as in Fig. 1. lb = lower basin, hw = headwater

Sample	Composition	Type of sample	pH	T	EC	CO_3^{-2}	HCO_3^-	Cl^-	SO_4^{-2}	Ca^{+2}	Mg^{+2}	Na^+	K^+	As	SI cal	SI gyp	SI hal
				(°C)	(µS cm^{-1})	(mg L^{-1})									(Dimensionless)		
1	Ca-HCO_3-SO_4	Stream	8.09	20.5	1386	0	130.6	255.1	445.7	111.2	22.6	124.0	44.0	0.263	0.59	−0.98	−6.12
2	Na-Cl	Stream	8.11	39.2	3830	0	118.4	837.4	407.1	88.2	13.4	590.0	81.0	0.883	0.42	−1.2	−4.96
3	Na-Cl	Stream	8.03	19.3	3200	18.84	92.3	814.3	110.0	88.5	14.8	330.0	77.0	0.865	0.32	−1.66	−5.2
4	Na-Cl	Stream	8.19	27.5	3800	12.84	95.3	932.0	111.9	92.0	11.9	400.0	86.0	0.922	0.49	−1.65	−5.07
5	Na-Cl	Stream	7.99	39.4	1952	0	163.7	1033.5	45.9	26.7	9.6	720.0	69.0	0.939	0	−2.57	−4.77
6	Ca-HCO_3-SO_4-Cl	Stream	8.04	15	817	0	138.4	60.0	106.4	102.0	22.4	29.0	7.5	0.069	0.66	−1.48	−7.35
7	Na-Cl	Stream	8.43	31.5	2980	11.13	112.3	616.0	100.9	79.2	13.4	230.0	61.0	0.650	0.76	−1.7	−5.47
8	Na-Cl	Stream	8.37	27.9	2770	12.8	90.5	643.6	82.5	79.8	13.4	320.0	64.0	0.649	0.61	−1.79	−5.31
9	Na-Cl	Stream	8.61	30	3060	6.85	100.1	687.4	88.0	53.1	15.5	350.0	67.0	0.698	0.7	−1.94	−5.24
10	Na-Cl	Stream	8.32	23.4	3100	0	111.4	710.5	80.7	68.0	7.2	270.0	66.0	0.733	0.59	−1.85	−5.34
11	Na-Cl	Stream	8.29	20.4	2370	0	110.6	592.9	60.5	56.6	11.8	290.0	53.0	0.584	0.5	−2.04	−5.38
12	Ca-SO_4	River	7.94	18.1	320	0	90.5	1.4	161.4	51.6	12.4	4.1	1.9	0.009	0.11	−1.51	−9.81
13	Na-SO_4-Cl	River	7.8	14.6	733	0	95.8	141.4	161.4	41.6	18.7	121.0	9.0	0.144	−0.14	−1.67	−6.36
14	Na-Cl	Thermal	8.8	67	9610	17.1	77.5	1801.6	289.8	17.7	11.1	1030.0	160.0	1.969	0.14	−2.1	−4.41
15	Na-Cl	Thermal	8.54	92.4	5490	12.9	82.7	1584.8	201.7	30.1	11.6	810.0	79.0	1.793	0.21	−1.97	−4.56
16	Na-Cl	Thermal	7.25	62.4	1485	0	108.4	998.9	45.9	9.5	8.3	470.0	55.0	0.960	−1.32	−2.95	−4.96
17	Na-Cl	Thermal	7.17	57.3	2840	0	148.9	615.9	150.4	9.2	5.4	510.0	37.0	0.647	−1.3	−2.45	−5.13
18	Na-Cl	Thermal	7.68	59.7	4480	0	99.2	1130.3	67.7	15.5	7.1	550.0	60.0	0.944	−0.75	−2.61	−4.85

(continued)

Table 1 (continued)

Sample	Composition	Type of sample	pH	T	EC	CO_3^{-2}	HCO_3^-	Cl^-	SO_4^{-2}	Ca^{+2}	Mg^{+2}	Na^+	K^+	As	SI cal	SI gyp	SI hal
				(°C)	($\mu S\ cm^{-1}$)	($mg\ L^{-1}$)									(Dimensionless)		
19	Na-Cl	Thermal	8.3	56.2	1561	0	106.2	1065.8	172.4	14.3	1.9	820.0	59.0	0.894	−0.19	−2.3	−4.71
20	Na-Cl	Thermal	7.64	55.8	1391	0	120.1	959.6	49.5	6.5	10.0	470.0	60.0	0.910	−1.06	−3.08	−4.98
21	Na-Cl	Thermal	7.37	40	1866	0	123.6	777.4	34.9	4.7	11.1	380.0	49.0	1.969	−1.43	−3.33	−5.15
22	Na-Cl	Thermal	9.34	66.1	8850	46.2	20.0	2507.5	108.2	15.8	11.6	1170.0	190.0	2.271	−0.12	−2.59	−4.22
23	Na-Cl	Thermal	8.63	60.1	6370	24.0	104.5	1831.6	64.2	34.8	13	910.0	95.0	1.754	0.46	−2.41	−4.45
24	Ca-HCO_3	Spring (hw)	7.44	8.2	39	0	59.2	5.6	4.6	9.6	2.8	5.4	0.6	0.01	−1.15	−3.54	−9.05
25	Ca-HCO_3	Spring (hw)	6.95	12	25	0	42.7	0.9	1.1	8.9	0.8	1.1	0.2	0.001	−1.79	−4.15	−10.53
26	Na-Cl	Spring (lb)	7.02	19	347	0	77.0	70.1	5.5	11.9	4.5	38.0	7.5	0.102	−1.4	−3.45	−7.12
27	Na-Cl	Spring (lb)	7.55	21.4	893	0	58.8	244.8	47.7	13.0	7.7	118.0	19.0	0.103	−1.04	−2.6	−6.12
28	Na-Cl	Spring (lb)	7.12	22.6	1741	0	89.7	512.6	16.7	3.1	11.5	250.0	6.9	0.298	−1.94	−3.75	−5.49
29	Na-Cl	Spring (lb)	6.76	nd	nd	0	54.0	79.1	4.6	10.2	1.8	38.0	9.1	0.052	−1.88	−3.57	−7.07

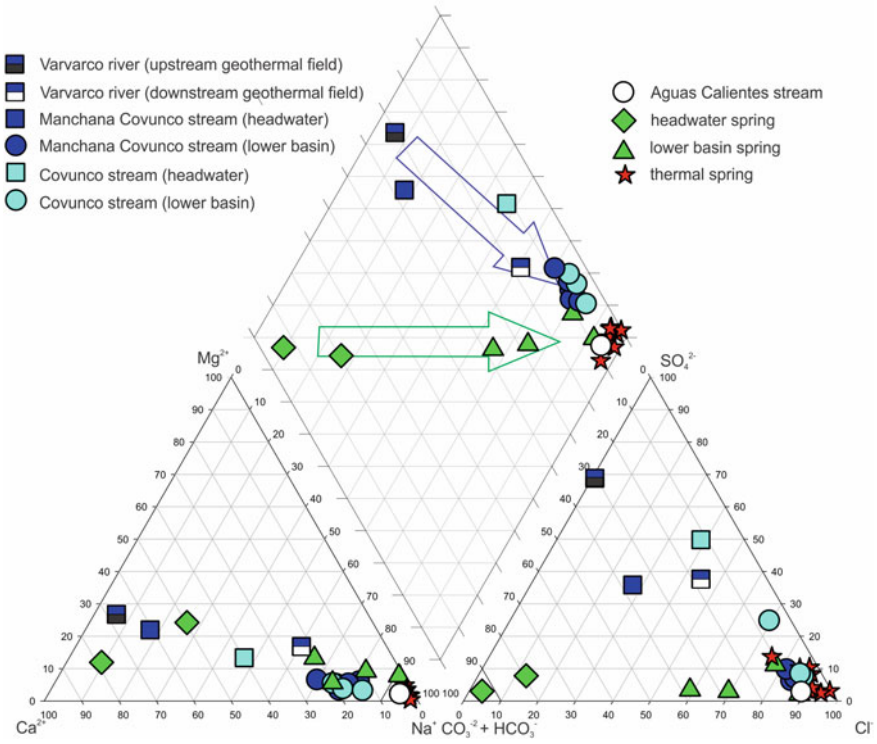

Fig. 3 Piper diagram showing the major composition and evolution of the studied waters. The blue arrow indicates the chemical evolution of stream water and the green arrow that of springs. Note that the symbol of the Aguas Calientes stream overlaps with thermal springs

both cases, the changing trend of chemical facies (towards Na-Cl compositions) is strongly controlled by the composition of the thermal springs.

On the other hand, thermal springs are characterized by high concentrations of As with values between 0.894 and 2.271 mg L^{-1} (Table 1). At headwaters low concentrations of As were measured (between 0.069 and 0.263 mg L^{-1}), while in the low basins, the streams present higher As values, between 0.584 and 0.939 mg L^{-1} (Table 1).

The analysis of the interaction between water and minerals (found in the rocks that compose the stream beds), performed by ionic relationships, allows the visualization of different behaviors (Fig. 4). The graph Na^+ versus Cl^- (Fig. 4a) shows that set of analyzed samples are grouped around the 1:1 ratio linear trend, which characterizes thermal springs, also showing higher concentrations of these ions. It is important to note that surface waters from Manchana Covunco and Covunco streams retrieved downstream and also the Aguas Calientes stream show a marked association with the thermal spring samples with respect to these ions. Besides, waters from the Varvarco River, although they are adjusted to the 1:1 ratio linear trend, they register low

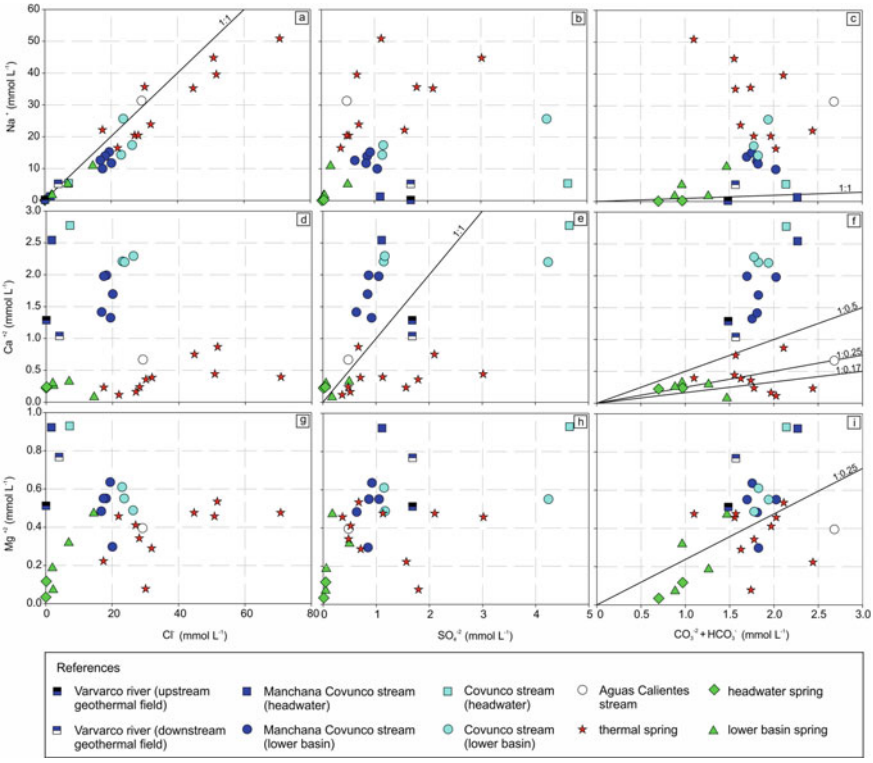

Fig. 4 Bivariate plots for each group of samples showing ionic relationships between anions and cations in mmol L^{-1}. The lines of theoretical dissolution of some minerals are also included

concentrations of these ions. The high Na^+ contents in the thermal springs determine that these samples (14–23, Fig. 1b) differ from the streams (with the exception of the Aguas Calientes sample) and the springs in the Na^+ versus SO_4^{-2} and Na^+ versus $CO_3^{-2} + HCO_3^-$ graphs (Fig. 4b–c).

The relationships Ca^{+2} versus Cl^-, Ca^{+2} versus SO_4^{-2} and Ca^{+2} versus $CO_3^{-2} + HCO_3^-$ show that thermal springs, springs, and the Aguas Calientes stream registered increases in its anionic contents associated with low concentrations of Ca^{+2} (Fig. 4d–f). Particularly, in the Ca^{+2} versus $CO_3^{-2} + HCO_3^-$ plot, the waters present ratios associated with the weathering of carbonates (1:0.5), oligoclase-type plagioclase (1:0.17), and pyroxenes (1:0.25). A different behavior is evidenced in samples from the Manchana Covunco and Covunco streams, where high Ca^{+2} concentrations are registered without observing a clear trend between the increase of this ion and the major anions. In the Ca^{+2} versus SO_4^{-2} graph, samples from the Varvarco River are close to the 1:1 ratio associated with the gypsum-anhydrite dissolution (Fig. 4e). Likewise, Mg^{+2} versus Cl^- and Mg^{+2} versus SO_4^{-2} graphs do not show trends in the different samples (Fig. 4g–h), whereas with respect to Mg^{+2} versus $CO_3^{-2} + HCO_3^-$ (Fig. 4i) the increase of these ions occurs in thermal springs, springs, and

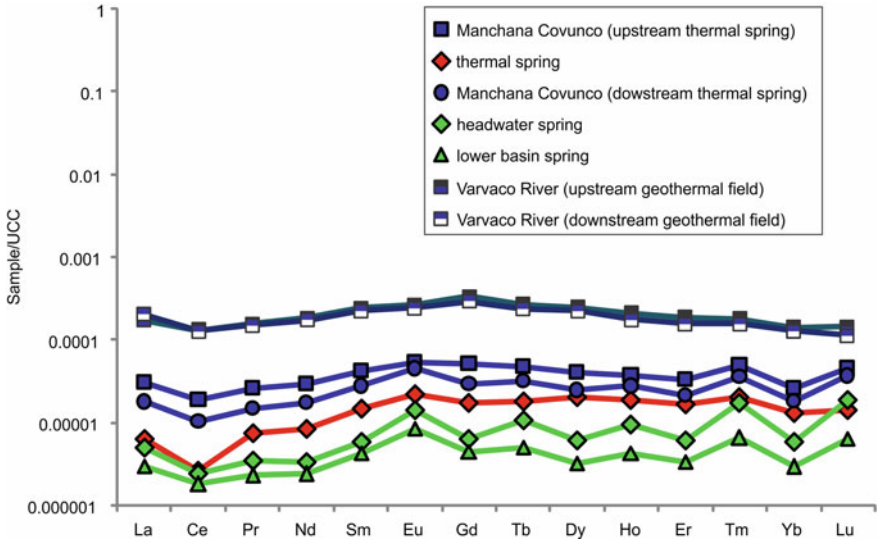

Fig. 5 Spider diagrams for dissolved rare earth elements (REE) normalized to Upper Continental Crust (UCC, McLennan 2001) for springs, streams, river and thermal spring from the studied system

Aguas Calientes stream with a ratio close to 1:0.25 corresponding to the weathering of pyroxenes.

The saturation indices (SI) with respect to calcite (Table 1) show subsaturated values for the springs waters, subsaturated to supersaturated for thermal springs and close to equilibrium to supersaturated in the streams and Varvaco River waters. The gypsum SI, although in all cases is negative (subsaturated), show a tendency towards equilibrium (less negative values) from springs to thermal springs and streams waters (Table 1). Regarding the halite SI, despite the high Cl^- and Na^+ concentrations registered in thermal springs, all samples presented subsaturated values, being more negative in springs and less negative in thermal springs waters (Table 1).

Some selected samples were analyzed in order to determine the concentration and variability of dissolved REE in the studied system. Five samples of the Manchana Covunco watershed, as well as, the two samples of the Varvaco River, were chosen for this purpose. Springs samples show the lowest total dissolved REE concentrations, with a ΣREE varying from 0.56 $\mu g\ L^{-1}$ at the headwaters to 0.36 $\mu g\ L^{-1}$ at the low basin. The analyzed thermal spring sample exhibits a ΣREE of 0.96 $\mu g\ L^{-1}$, whereas the Manchana Covunco stream shows a decreasing total dissolved REE content downstream the thermal spring, since in this river the ΣREE varies from 3.9 (upstream) to 2.3 $\mu g\ L^{-1}$ (downstream). On the other hand, the Varvarco River REE concentrations are of an order of magnitude higher than those of the other analyzed waters, and the river evidences almost no variation in the ΣREE from the headwaters to the low basin.

Figure 5 shows the spider diagram of the dissolved REE normalized to the Upper Continental Crust (UCC, McLennan 2001) for the studied system. The water samples

present REE concentrations of about 10^4 to 10^7 times lower that of the UCC. In the Manchana Covunco watershed the samples show, in general, similar UCC-normalized distribution, with relatively flat patterns and without evidence of significant fractionation between light (LREE, among La-Sm) and heavy (HREE, among Gd-Lu) rare earths elements ($La_N/Yb_N \sim 1$). An exception is given by the thermal spring that exhibits HREE-enriched UCC-normalized concentrations ($La_N/Yb_N = 0.48$). Besides, all samples of the Manchana Covunco basin present a negative Ce anomaly, and a positive Eu anomaly, the latter is more pronounced in springs. Positive $(Eu/Eu^*)_N$ in waters are usually attributed to the preferential weathering of plagioclase, because Eu^{+2} may substitute Sr^{+2} or Ca^{+2} in Ca-plagioclase (e.g. McLennan 1989). Meanwhile, negative Ce anomaly is due to the oxidation of Ce^{+3} to Ce^{+4} under alkaline conditions, which decreases its solubility and promotes its precipitation (e.g. Elderfield et al. 1990). The Varvaco River samples show a different UCC-normalized pattern, characterized by a barely enrichment in the LREE (mean $La_N/Yb_N = 1.41$) and a slightly negative Eu anomaly (mean $Eu/Eu^* = 0.93$).

4 Hydrogeochemical Processes and Geothermal Influence on Streams

The chemical characteristics of water along the streams highlight the clear influence that geothermal discharges have on them. Most of the **meltwater** infiltrates and recharges the groundwater which then forms the springs, and another part of this melting water drains feeding the streams (Tassi et al. 2016; Villalba et al. 2020). At the headwater area, upstream the geothermal field, the temperature of springs and streams (samples 1, 6, 24 and 25) are close to 13.9 °C. This value is strongly influenced by the climatic conditions, being similar to the average annual temperature recorded in the area (Pesce 2013). Streams and springs are characterized by neutral to slightly alkaline pH conditions, low EC, and Ca-HCO_3-SO_4 facies. The predominance of Ca^{+2}, HCO_3^- and SO_4^{-2} ions would be related mainly to the alteration of the mudstones and sandstones with a carbonate matrix, and gypsum that dominates headwaters area (Zanettini et al. 2001). In particular, stream waters present the highest Ca^{+2} concentrations and they are supersaturated with respect to calcite. The presence of gypsum that accompanies these sedimentary rocks would be an extra source of Ca^{+2}, and it would also contribute SO_4^{-2} ions, mainly in the Manchana Covunco stream (Fig. 4e). Although those waters are subsaturated with respect to gypsum, they show the least negative SI values regarding this mineral (Table 1). It is relevant to note that in this sector the high SO_4^{-2} contents in some samples could be also explain by the oxidation processes of H_2S at shallow depth (Tassi et al. 2016). At the springs, calcite and gypsum SI show subsaturation associated with low Ca^{+2} concentrations, despite this is the dominant cation. In the springs, the ionic relationships also indicate contributions of Ca^{+2}, Mg^{+2}, and HCO_3^- from the dissolution of silicates, such as plagioclase and pyroxenes (Figs. 4f and i). On the other hand, the

dissolution of albite (Fig. 4c) contributes Na^+ and HCO_3^- ions to both, springs and stream waters.

This hydrochemical signature of stream waters and springs in the headwaters sector strongly contrasts with that of the thermal springs. All thermal springs are characterized by high temperature (greater than 40.0 °C), relatively high EC (up to 1866.0 $\mu S\ cm^{-1}$) and by the dominance of Na-Cl facies. High concentrations of Na^+ and Cl^- are consistent with mature waters of geothermal systems at high temperatures. The concentrations of Na^+ and Cl^- were stoichiometrically equivalent as expected for typical geothermal brines (Giggenbach 1997; Vengosh et al. 2002). Gases such as SO_2 and HCl from the magmatic source dissolve within the hydrothermal groundwater to produce SO_4^{-2} and Cl^- (Tassi et al. 2016). As mentioned before, this SO_4^{-2} contribution would also explain the deviation of thermal spring waters in the graph of Ca^{+2} versus SO_4^{-2} (Fig. 4e). Likewise, it is expected that the contributions of Ca^{+2}, Mg^{+2} and HCO_3^- derive from the underlying igneous rocks (Zanettini et al. 2001). Given that aqueous emissions are the product of deep convective circulation of meteoric water (Panarello et al. 1992), most geochemical features of thermal springs would be acquired in depth. Extra contributions of HCO_3^- can also come from the dissolution of $CO_{2(g)}$ since this gas is one of the main components of the **fumaroles** (Tassi et al. 2016). However, saturated values in calcite are recorded, which would be the responsible of the precipitation of carbonatic terraces located in the vicinity of the thermal springs (Polk 1994; Villalba et al. 2020).

The low flow rates of streams (mean of 0.81 $m^3\ s^{-1}$) determine that the contributions from thermal springs strongly modified the chemical characteristics of stream waters. Downstream thermal springs, stream waters increase their EC and show the dominance of Na-Cl facies (Figs. 3 and 4). The contribution from thermal springs is registered not only in the facies change, but also in the Na^+ versus Cl^- ratio. With the purpose of estimating the contribution of thermal springs onto stream waters and springs downstream the geothermal field, an end-member mixing analysis was performed using chloride concentration as the dominant conservative ion of thermal springs. In the case of surface water streams, Cl^- concentration in the headwaters of the watershed and the average Cl^- concentration in thermal springs were considered as end members. As for springs, Cl^- concentration of the headwaters of the watershed and the average Cl^- concentration in thermal springs were considered.

The theoretical mixing model using Cl^- concentrations, allowed the estimation of the influence of thermal springs in the chemistry of stream and spring waters. The obtained results are schematically summarized in Fig. 6. For the Manchana Covunco watershed, the selected end-members were the sample from headwaters (sample 1) and the average concentration of Cl^- of the thermal springs (samples 14 and 15). It was estimated that downstream (sample 4), the contribution from thermal springs is of 47%. For the Covunco watershed case, the chosen end-members were a surface water sample located at the headwaters (sample 6) and the average concentration of Cl^- of thermal springs of the same water course (samples 22 and 23), estimating that downstream (sample 11), the water shows a 24% of geothermal contribution. At Aguas Calientes stream, no mixtures were calculated since, as it was observed in the chemical facies and ionic relationships, it has a chemical signature dominated

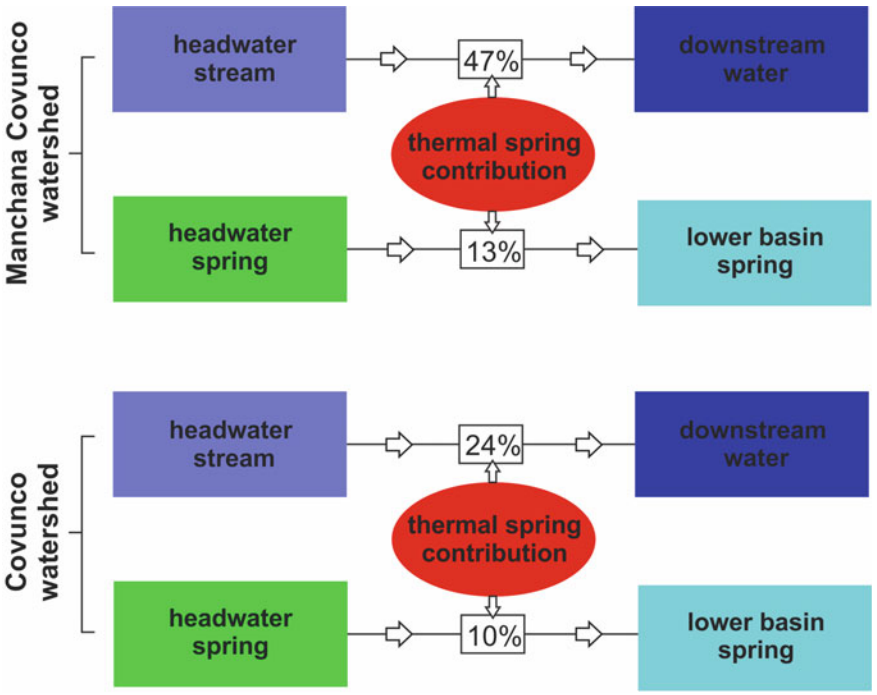

Fig. 6 Schematic diagram showing the estimated contributions of the thermal springs on the stream and spring waters in the downstream watershed of the Domuyo geothermal field

by thermal springs. In the case of springs, a mixture was computed between the Cl^- concentration of samples 24 and 25 (springs from headwaters) with the average concentration of Cl^- of thermal springs (samples 14 and 15, Manchana Covunco watershed) for the first case, and samples 22 and 23 (Covunco watershed) for the second one, estimating that downstream the springs, the geothermal contribution is between 10 and 13%.

The contribution from thermal springs with low Ca^{+2} concentrations produces an overall decrease in the Ca^{+2} contents from the headwaters to the lower basin due to the effect of dilution (Fig. 4d–f). In Manchana Covunco and Covunco streams there is an excess of Ca^{+2} which could be attributed to cation exchange processes, where the dominance of Na^+ would displace Ca^{+2} from the adsorption surface, constituting an extra contribution of this ion to the waters. The presence of adsorbent minerals such as clays and zeolites, associated with the adjacent areas to the geothermal field (Mas et al. 2000), would support the occurrence of this process.

Regarding trace elements concentrations that can limit the water quality for human consumption, it was observed that thermal springs also influence the concentrations of these elements. The elevated concentration of As recorded in thermal spring waters evidences how the interaction between rocks and waters at high temperature mobilizes As (Ellis and Mahon 1964, 1967). Considering the water quality standards

(WHO 2008), the geothermal contribution of As determines the potability of springs and stream waters located in the lower basin. Comparing the concentration of this trace element determined for headwaters and lower basin areas, it is evident that thermal springs deteriorate water quality for human supply. Thermal springs increase the As content to ~ 0.139 mg L^{-1} in the lower basin samples (Villalba et al. 2020).

The influence of thermal springs on the Manchana Covunco stream is also evidenced in the geochemistry of dissolved REE. Thermal spring waters have lower REE concentrations than stream surface waters at the headwaters, which are reflected in the decrease in total REE contents downstream. Moreover, the LREE/HREE fractionation as well as the positive Eu anomaly and negative Ce anomaly also show the influence of thermal springs on streams. On the other hand, the Aguas Calientes stream, which is mainly fed by thermal springs, has a major composition remarkably similar to that of thermal springs (Figs. 3 and 4). Note that the contribution from thermal springs is also recorded in springs, with an average percentage of 10% (Fig. 6). The influence of thermal springs on springs and water streams of the Domuyo System Natural Protected Area is outlined in Fig. 7. The aforementioned figure is a summarized diagram of the hydrothermal system behavior based on the models postulated by numerous works carried out in the area from geological, geochemical, geophysical, and satellite data (e.g. Panarello et al. 1992; JICA 1983–1984; Galetto et al. 2018; Tassi et al. 2016; Astort et al. 2019; Villalba et al. 2020).

The streams described above drain towards the Varvarco River, which has a higher flow, with discharges close to 94 m^3 s^{-1} (FAO 2015). This large difference in flow

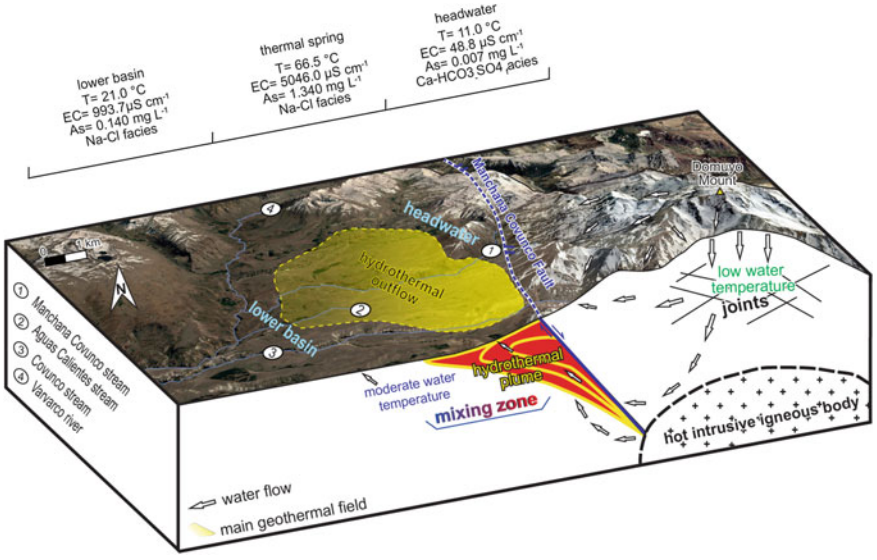

Fig. 7 Conceptual model summarizing the hydrochemical variations observed due to the interaction between the geothermal system studied and the different water streams and springs at the western slopes of the Domuyo Mount

rates, almost two orders of magnitude greater than the studied streams, may suggest that no significant variations in the chemical signature may be expected. However, a slight contribution of Na^+ and Cl^- ions can be detected in the Varvarco River downstream the geothermal field, which can be explained by the chemical facies observed in thermal springs (Figs. 3 and 4a). Upstream the geothermal field, the Varvarco River waters present Ca-SO_4 facies saturated in calcite and subsaturated in gypsum, whose composition would be mainly associated with the contribution of evaporitic rocks, like carbonates and gypsum, rocks outcropping in the upper basin (Zanettini et al. 2001). Downstream the geothermal field, the Varvarco River waters are of the Na-SO_4-Cl type, subsatured in calcite and gypsum and with a tendency to increase in Na^+ and Cl^- concentrations, similar to that of thermal springs, which may indicate its influence in the river chemistry. However, and possibly due to its low dissolved concentrations, both, the Na^+ and Cl^- contents and the distribution patterns of REE, do not show significant modifications in the Varvarco River downstream the geothermal field.

Despite the fact that there are no large populations in the study area, there are small family settlements and also nomadic people who raise livestock, as well as a small village that receives tourists (Aguas Calientes Village, Fig. 1). Thus, chemistry variations resulting from geothermal contribution acquire relevance in the area because stream waters and springs are the only source of water supply for local inhabitants. Although in this system changes associated with major ions and REE have been particularly analyzed, as it was stated above, thermal springs also provide trace elements such as As, which concentrations may cause geogenic contamination of water supply (Villalba et al. 2020), a characteristic that also affects other arid regions around the world (e.g. Ballantyne and Moore 1988; Smedley and Kinniburgh 2002; López et al. 2012).

5 Perspectives and Future Work

Streams and springs of the Domuyo geothermal field are the main sources of water supply for the local inhabitants (small family settlements and Aguas Calientes Village, Fig. 1) in this arid zone of northern Patagonia. In addition, these water courses are tributaries of the Varvarco River, from which small towns, such as Varvarco (60 km to the south) use water as a downstream supply. Therefore, a key aspect to analyze moving forward is the monitoring of changes in water quality over time due to changes in the dynamics of the Domuyo geothermal system and the variations of the recharge rate as a result of seasonal and long term climate changes. Additionally, further work is needed to articulate the research efforts with the local authorities in order to implement efficient water management policies in this remote area.

Acknowledgements This work was carried out thanks to the permits provided by Protected Natural Areas of the Province of Neuquén. Funding for this research was provided by the Agencia Nacional

de Promoción Científica y Tecnológica (PICT 2014-2206 and PICT 2019-4086) and the Consejo Nacional de Investigaciones Científicas y Técnicas (CONICET).

References

Agusto MR (2011) *Estudio geoquímico de los fluídos volcánicos e hidrotermales del Complejo Volcánico Copahue-Caviahue y su aplicación para tareas de seguimiento.* Doctoral thesis. Facultad de Ciencias Exactas y Naturales, Universidad de Buenos Aires (in Spanish)

Astort A, Walter TR, Ruiz F, Sagripanti L, Nacif A, Acosta G et al (2019) Unrest at Domuyo volcano, Argentina, detected by geophysical and geodetic data and morphometric analysis. Remote Sens 11(18):2175

APHA American Public Health Association (2015) Standard methods for the examination of water and wastewater. American Water Works Association, Water Environment Federation, Washington, DC

Ballantyne JM, Moore JN (1988) Arsenic geochemistry in geothermal systems. Geochim Cosmochim Acta 52(2):475–483

Burd AI, Booker JR, Mackie R, Favetto A, Pomposiello MC (2014) Three-dimensional electrical conductivity in the mantle beneath the Payún Matrú Volcanic Field in the Andean backarc of Argentina near 36.5 S: Evidence for decapitation of a mantle plume by resurgent upper mantle shear during slab steepening. Geophys J Int 198(2):812–827

Chiodini G, Liccioli C, Vaselli O, Calabrese S, Tassi F, Caliro S et al (2014) The Domuyo volcanic system: an enormous geothermal resource in Argentine Patagonia. J Volcanol Geotherm Res 274:71–77

Cogliati MG, Ostertag G, Caso M, Finessi FG, Groch D (2018) Análisis del balance hídrico medio mensual en la provincia del Neuquén (Argentina). Boletín Geográfico 40(2):26–44 (in Spanish)

Elderfield HR, Upstill-Goddard R, Sholkovitz ER (1990) The rare earth elements in rivers, estuaries and coastal sea waters: processes affecting crustal input of elements to the ocean and their significance to the composition of seawater. Geochim Cosmochim Acta 54:971–991

Ellis AJ, Mahon WAJ (1964) Natural hidrothermal systems and experimental hot-water/rock interactions. Geochim Cosmochim Acta 28:1324–1367

Ellis AJ, Mahon WAJ (1967) Natural hydrothermal systems and experimental hot-water/rock interactions. Geochim Cosmochim Acta 31:519–538

FAO Food and Agriculture Organization (2015) Documento de Trabajo N°7B: Balance Hídrico de la Cuenca del río Neuquén, Provincia del Neuquén. http://www.fao.org/fileadmin/user_upload/rlc/utf017arg/neuquen/DT_07B_Balance_HC3ADdrico_Cuenca_Neuquen.pdf. Accessed 13 July 2020 (in Spanish)

Galetto A, García V, Caselli A (2018) Structural controls of the Domuyo geothermal field, Southern Andes (36 38′ S), Argentina. J Struct Geol 114:76–94

Giggenbach WF (1997) The origin and evolution of fluids in magmatic-hydrothermal systems. In: Barnes HL (ed) Geochemistry of hydrothermal ore deposits. John Wiley and Sons, New York, pp 737–796

JICA Japan International Cooperation Agency (1983–1984) Ente Provincial de Energía de Neuquén, JICA-EPEN. Argentine Republic. Final Report on the Northern Neuquén Geothermal Development Project, 126

López DL, Bundschuh J, Birkle P, Armienta MA, Cumbal L, Sracek O et al (2012) Arsenic in volcanic geothermal fluids of Latin America. Sci Total Environ 429:57–75

Mas GR, Bengochea L, Mas LC (2000) Hydrothermal alteration at El Humazo Geothermal area, Domuyo Volcano, Argentina. In: Proceedings of the World Geothermal Congress, Kyushu, Tohoku, Japan, pp 1413–1418

Mas LC (2010) History and Present Situation of the Neuquén Geothermal Project. In: Proceedings of World Geothermal Congress. Bali, Indonesia

McLennan SM (1989) Rare earth elements in sedimentary rocks: influence of provenance and sedimentary processes. In: Lipin BR, McKay GA (eds) Geochemistry and mineralogy of rare earth elements, reviews in mineralogy, vol 21. Mineralogical Society of America, Washington D.C., pp 169–200

McLennan SM (2001) Relationships between the trace element sedimentary rocks and upper continental crust. Geochem Geophys Geosyst 2(4): 2000GC000109

Miranda F, Folguera A, Leal PR, Naranjo JA, Pesce A (2006) Upper Pliocene to lower Pleistocene volcanic complexes and upper Neogene deformation in the south-central Andes (36 ° 30 '-38 °S). Geol Soc Am Spec Pap 407:287

Monasterio AM, Armijo F, Hurtado I, Maraver F (2017) Análisis de las aguas minerales de la Provincia del Neuquén, República Argentina. Bol Soc Esp Hidrol Med 32(1):117–118

Panarello H, Sierra JL, Pedro G, D'Amore F (1992) Isotopic and geochemical study of the Domuyo Geothermal field. Neuquén, Argentina (N° IAEA-TECDOC-641)

Parkhurst DL, Appelo C (1999) User's guide to PHREEQC (Version 2): a computer program for speciation, batch-reaction, one-dimensional transport, and inverse geochemical calculations. Water-Resour Inv Rep 99(4259):312

Pesce AH (2013) The Domuyo Geothermal Area, Neuquén, Argentina. Geotherm Resour Council Trans 37:309314

Piper AM (1944) A graphic procedure in the geochemical interpretation of water analyses. Am Geophys Union Trans 25

Polk RE (1994) Interaction between bacteria, nanobacteria, and mineral precipitation in hot-springs in central Italy. Géogr Phys Quat 48:233–246

Smedley PL, Kinniburgh DG (2002) A review of the source, behaviour and distribution of arsenic in natural waters. J Appl Geochem 17(5):517–568

Smiler R (2009) Diagrammes software. Logiciel libre du laboratoired 'Hydrogéologie, universitéd' Avignon. http://www.lha.univavignon.fr/LHA-Logiciels.htm. Accessed 20 July 2020

Tassi F, Liccioli C, Agusto M, Chiodini G, Vaselli O, Calabrese S et al (2016) The hydrothermal system of the Domuyo volcanic complex (Argentina): a conceptual model based on new geochemical and isotopic evidences. J Volcanol Geotherm Res 328:198–209

Vengosh A, Helvacı C, Karamanderesi IH (2002) Geochemical constraints for the origin of thermal waters from western Turkey. J Appl Geochem 17(3):163–183

Villalba E, Tanjal C, Borzi G, Páez G, Carol E (2020) Geogenic arsenic contamination of wet-meadows associated with a geothermal system in an arid region and its relevance for drinking water. Sci Total Environ 137:571

WHO World Health Organization (2008) Guidelines for drinking-water quality: second addendum, vol 1, Recommendations

Zanettini JC, Santamaría GR, Leanza HA (2001) Hoja de la Carta Geológica de la República Argentina E. 1: 250.000 num. 3772-II (Las Ovejas) Provincia del Neuquén. Instituto de Geología y Recursos Minerales, Servicio Geológico Minero Argentino. Secretaría de Minería, Argentina. Boletín 263 (in Spanish)